nature photonics

ARTICLES

https://doi.org/10.1038/s41566-018-0113-8

Single-shot measurement of phase and amplitude by using a heterodyne time-lens system and ultrafast digital time-holography

Alexey Tikan[1,2], Serge Bielawski[1,2], Christophe Szwaj[1,2], Stéphane Randoux[1,2] and Pierre Suret[1,2]*

Temporal imaging systems are outstanding tools for single-shot observation of optical signals that have irregular and ultrafast dynamics. They allow long time windows to be recorded with femtosecond resolution, and do not rely on complex algorithms. However, simultaneous recording of amplitude and phase remains an open challenge for these systems. Here, we present a new heterodyne time-lens arrangement that efficiently records both the amplitude and phase of complex and random signals over large temporal windows (tens of picoseconds). Phase and time are encoded onto the two spatial dimensions of a camera. We implement this phase-sensitive time-lens system in two configurations: a time microscope and a digital temporal-holography device that enables single-shot measurement with a temporal resolution of ~80 fs. We demonstrate direct application of our heterodyne time-lens to turbulent-like optical fields and optical rogue waves generated from nonlinear propagation of partially coherent waves inside optical fibres.

Simultaneous measurement of the amplitude and phase of ultrafast complex optical signals is a key question in modern optics and photonics[1–7]. This kind of detection is needed for the characterization of various fundamental phenomena such as supercontinuum[8,9], optical rogue waves[10–12] or soliton dynamics in mode-locked lasers[13,14]. The task remains a particularly challenging open problem when femtosecond resolution and long time windows are simultaneously required. These requirements are found, for example, in the context of nonlinear statistical optics, for the characterization of random light[15] or in the study of spatiotemporal dynamics of continuous-wave lasers[16].

In the quest for long-window and ultrafast recording tools, temporal imaging devices, such as time lenses, are considered as promising candidates. Time lenses enable femtosecond time evolutions to be manipulated so that they can be magnified in time[17–20] or spectrally encoded[11,18,21] with high fidelity. These replica of the signal evolutions can thus be recorded using a simple gigahertz oscilloscope (for time-magnification systems) or a single-shot optical spectrum analyser[11]. No special algorithms are necessary for retrieving the ultrafast power evolutions, long windows can be recorded (up to hundreds of picoseconds) and the method is suitable for recording continuous-wave (that is, non-pulsed) complex signals. Recently, temporal imaging systems have thus begun to play a central role in fundamental studies dealing with nonlinear propagation of light in fibres leading, for example, to the emergence of rogue waves and integrable turbulence[11,12], a field of experimental research where recording long temporal traces with femtosecond resolution is mandatory.

However, a range of applications is still hampered by the need to also record the phase evolution of long and complex ultrafast optical signals. Extension of temporal imaging has been performed in this direction, by performing heterodyning in temporal magnification systems[22,23], that is, for which the readout is performed using a single-pixel photodetector. However, these systems have not demonstrated subpicosecond capability.

Here we show that temporal imaging systems can be transformed in a full amplitude and phase digitizing device, without trade-off on femtosecond resolution and size of recording window. The principle is to use a spectral-encoding time lens, which encodes the time evolution onto the horizontal axis of a camera, and obtain the phase information by performing heterodyning on the other (vertical) direction. This spatial encoding arrangement is comparable to strategies used in two-dimensional (2D) interferometry, SEA-TADPOLE[4], SEA-SPIDER[24,25] and STARFISH[5], except that we directly image the time evolution (instead of a spectrum) on the camera.

We present a versatile set-up that can be used in two configurations named heterodyne time microscope (HTM) and spatial encoding arrangement with hologram observation for recording in single shot the electric field (SEAHORSE). In the HTM, the focus is achieved by using an (analog) optical dispersive element, as in conventional time-lens devices. In contrast, the determination of the amplitude and of the phase by SEAHORSE is analogous to digital holography and thus requires ex post data analysis in which the focus operation is achieved in a numerical way.

Using the HTM, we report original experimental observations of the amplitude and phase fluctuations of the random light delivered by an amplified spontaneous emission (ASE) light source. Then, we investigate the question of nonlinear propagation of random light in optical fibres. Finally, by measuring double femtosecond pulses, we demonstrate that the SEAHORSE can be used to significantly decrease the aberrations inherent to all time-lens devices. We conclude by briefly comparing the HTM and SEAHORSE.

Results

Experimental strategy of the HTM. Our experimental set-up for the measurement of phase and amplitude is shown in Fig. 1a and a detailed three-dimensional enlarged view of the heterodyne time lens is shown in Fig. 1b.

The time lens (that is, the temporal quadratic phase[17]) is provided by noncolinear sum frequency generation (SFG) inside a $\chi^{(2)}$

[1]Laboratoire de Physique des Lasers, Atomes et Molecules, UMR-CNRS 8523, Université de Lille, Villeneuve-d'Ascq, France. [2]Centre d'Etudes et de Recherches Lasers et Applications (CERLA), Villeneuve-d'Ascq, France. *e-mail: pierre.suret@univ-lille1.fr

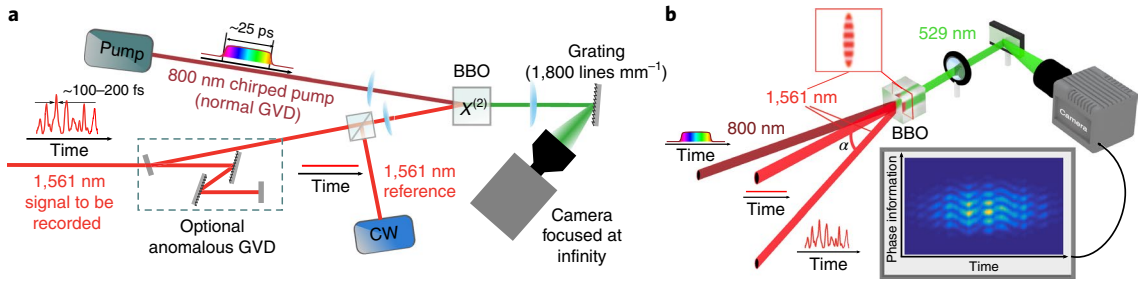

Fig. 1 | Heterodyne time-lens arrangement for amplitude and phase measurement of arbitrary signals. a, Complete set-up. The 'time lens' is provided by noncolinear SFG between the optical signal ($\lambda_S \cong 1{,}561$ nm) and a pump chirped pulse ($\lambda_P \cong 800$ nm) in a BBO crystal. The spectrum of the 529 nm SFG output is imaged onto the horizontal axis of a sCMOS camera by using a diffraction grating. In the HTM, the focus is achieved by using a Treacy compressor (optional anomalous GVD). In the SEAHORSE (temporal holography), the Treacy compressor is removed and the focus is achieved a posteriori by using numerical processing. Interference with the reference CW local oscillator (at $\lambda_R \cong \lambda_S$) produces horizontal fringes that are used to retrieve the phase information. **b**, Detailed view of the set-up. In the BBO crystal, all the beams have elliptic transverse shape. The CW local oscillator enters the crystal with a small vertical angle $\alpha \cong 10$ mrad. Note the typical 2D pattern recorded by using the camera: the horizontal axis corresponds to the time evolution and the vertical position of the fringes corresponds to the phase.

beta barium borate (BBO) crystal between the signal field with a central wavelength $\lambda_S \cong 1{,}561$ nm and a chirped pump pulse having a central wavelength $\lambda_P \cong 800$ nm.

Measurement of the optical phase is achieved from an heterodyne set-up based on the beating between the signal beam and a reference single-frequency laser emitting at a fixed wavelength $\lambda_R = 1{,}561$ nm. The reference beam reaches the BBO crystal by making a small vertical angle $\alpha \cong 10$ mrad with respect to the incidence plane that contains the pump beam and the signal beam. This produces an interference pattern at a wavelength $\lambda \cong 1{,}561$ nm that is copied at a shorter wavelength $\lambda_{vis} \cong 529$ nm by the process of SFG. The spectrum of the light generated at λ_{vis} is imaged onto the horizontal axis of a scientific complementary metal–oxide–semiconductor (sCMOS) camera by using a simple diffraction grating (see Methods).

The focus of the HTM is achieved by carefully tuning the dispersion experienced by the random signal light in a Treacy grating compressor (see the optional dispersive element displayed on Fig. 1a, Methods and refs [11,17–19]). The power distribution along the horizontal axis is then a replica of the input signal power evolution and the device is similar in its principle to the time microscope reported in ref. [11] where time is encoded into space.

In the vertical direction, the position of the fringes of interference (that is, for example, the position of the maxima of the interference pattern) is directly proportional to the relative phase $\phi(t)$ between the signal under investigation and the monochromatic reference field (see Methods). As a consequence, it is straightforward to extract the phase information from the pattern recorded in a single shot by the camera: the horizontal change in the vertical position of the fringes of interference directly provides the ultrafast evolution of the phase of the signal (Fig. 1b).

Our set-up provides single-shot snapshots of the phase and the amplitude of the signal over time windows with a width of around 40 ps. Those single-shot recordings are synchronized with the pump laser, at 1 kHz repetition rate (see Methods).

Application of the HTM to the analysis of a partially coherent light source. We now demonstrate how the HTM can be used to investigate phase and amplitude fluctuations of random light. We first investigate the partially coherent waves emitted by an ASE light source at a wavelength $\lambda \cong 1{,}561$ nm (see Methods). Using a programmable optical filter, the optical spectrum of the partially coherent light is designed to assume a Gaussian shape with a full width at half maximum $\Delta\nu$ that can be adjusted to some selected values.

Typical 2D beating patterns recorded in single shots by using the camera are shown in Fig. 2a,b while the retrieved phase $\phi(t)$ and the optical power fluctuations $P(t)$ are shown in Fig. 2c–f for $\Delta\nu = 0.1$ THz and $\Delta\nu = 0.7$ THz, respectively (see also Supplementary Video 1).

In the HTM, the retrieval algorithm for phase $\phi(t)$ and power $P(t)$ is very simple and straightforward. We call ϕ_S the phase of the signal. The phase ϕ_R of the reference laser can be considered as constant over each ~40-ps-long temporal window of measurement (see Methods). For each value of t (that is, for each vertical line of the pattern), the relative phase $\phi(t) = \phi_S(t) - \phi_R$ is given by the position of the maxima and is determined by using a procedure similar to the one described in ref. [26]. Note that we have controlled the calibration of our phase measurements by using monochromatic signals (see Supplementary Information). The optical power fluctuations $P(t)$ of the signal are simply computed from sums of intensities along vertical lines of the 2D patterns and from the knowledge of the reference profile recorded in another annex experiment (see Methods).

As expected, both the phase and the power of the ASE light randomly fluctuate over timescales of the order of the inverse of the spectral bandwidth, that is, $1/\Delta\nu \cong 10$ ps (Fig. 2c,e) and $1/\Delta\nu \cong 1$ ps (Fig. 2d,f). The typical amplitude of the phase excursion that is observed in our temporal window of 40 ps is directly related to the spectral bandwidth of the partially coherent light. From additional experiments with a pulsed laser, the temporal resolution of our HTM is found to be around 200 fs (see Supplementary Information).

Furthermore, a stringent test of the HTM can also be performed by comparing the optical spectrum deduced from the data with the optical spectrum recorded independently using an optical spectrum analyser (OSA). For each frame (recorded every millisecond), we compute the Fourier transform $\tilde{\psi}(\omega)$ of the complex envelope $\psi(t) = \sqrt{P(t)}\, e^{i\phi(t)}$ of the electric field measured by our HTM (ω being the angular frequency). Second, the mean Fourier power spectrum $\langle |\tilde{\psi}(\omega)|^2 \rangle$ of the partially coherent light is computed from an average ensemble that is made over 10^4 frames. The spectral power densities computed with this procedure for the ASE light with spectral widths $\Delta\nu = 0.1$ THz and $\Delta\nu = 0.7$ THz are plotted with red stars in Fig. 2g,h, respectively. In both cases, the spectral power density of the ASE light separately recorded with an OSA is plotted with a black line. The agreement between the spectra computed from the data recorded by the HTM and the spectra recorded with the OSA is remarkably good. These experiments with ASE light demonstrate that our HTM is indeed able to perform the accurate single-shot simultaneous measurement of phase and power of partially coherent waves fluctuating over subpicosecond timescales.

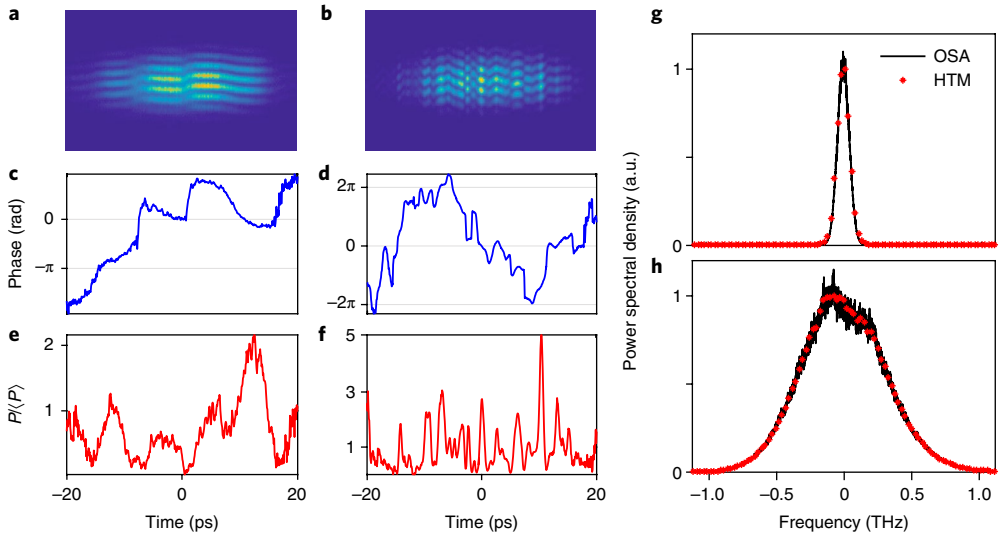

Fig. 2 | Phase, amplitude and spectrum of partially coherent waves (ASE). a–f, The width $\Delta\nu$ of the (average) optical spectrum of the partially coherent light waves emitted by an ASE source is adjusted by using a programmable filter. Results correspond to $\Delta\nu = 0.1$ THz (**a**,**c**,**e**,**g**) and $\Delta\nu = 0.7$ THz (**b**,**d**,**f**,**h**). **a**,**b**, Typical raw images recorded by the sCMOS camera of the HTM for ASE light with a spectral width $\Delta\nu = 0.1$ THz (**a**) and $\Delta\nu = 0.7$ THz (**b**). **c**,**d**, Phase retrieved from the interference pattern. **e**,**f**, Optical power normalized to the average power. In contrast to the raw signal in **a** and **b**, the signal in **e** and **f** is divided by the average power ($P(t)/\langle P\rangle$). **g**,**h**, Optical spectra corresponding to $\Delta\nu = 0.1$ THz and $\Delta\nu = 0.7$ THz, respectively. Red stars represent the spectrum computed from the averaged Fourier transform of the envelope of the electric field recorded with the HTM. The spectrum recorded by the OSA is plotted with black lines for comparison.

Observation of optical rogue waves and Peregrine soliton in nonlinear random waves (integrable turbulence) using HTM. Now we use the specific capabilities of our HTM to investigate the fundamental properties of nonlinear random waves. More precisely, we study the complex spatiotemporal structures that emerge from nonlinear propagation of partially coherent waves in optical fibres.

The principle of the experiments is represented in Fig. 3a. The partially coherent waves emitted by the ASE light source and spectrally filtered ($\Delta\nu = 0.1$ THz) are launched into a 400-m-long polarization maintaining fibre (PMF). The regime of dispersion is anomalous (focusing) and the average power of the ASE light propagating inside the PMF is $\langle P\rangle \simeq 2.6$ W.

Figure 3b–e represents the typical time evolutions of phase and amplitude that are observed at the output of the PMF by using our HTM (see also Supplementary Video 1). As already reported in refs [11,27], the optical power fluctuations at the output of the fibre exhibit extreme events or rogue waves with peak powers typically exceeding ten times the average power $\langle P\rangle$ and a short timescale (~500 fs).

Our experiments are well described by the integrable one-dimensional nonlinear Schrödinger equation (1D-NLSE) and thus fall within the framework of the so-called integrable turbulence[11,27–30] first introduced by Zakharov[31]. Numerical simulations of the focusing 1D-NLSE are performed by using random initial conditions (Methods for details). Remarkably, similar dynamical features are found to typify the phase and the amplitude evolutions both in experiments and in numerical simulations. We were in particular able to find some numerical realizations that closely resemble the experimental snapshots (compare Fig. 3b–e and f–i).

From our observations, several characteristics typifying the electric field at the output of the fibre can be pointed out both in experiments and in numerical simulations:

(1) The maxima of the amplitude often coincide with minima or maxima of the phase (Fig. 3b,c,f,g). This noticeable correlation arises from the nonlinear propagation and is not found in the initial random waves.
(2) In the parameters used here, the phase remains more or less bounded between 0 and 2π over the temporal windows of 40 ps (Fig. 3b–i).
(3) Numerous pulses with short duration and high peak power exhibit amplitude and phase profiles similar to those of the Peregrine soliton[32,33] (Fig. 3e,i). These pulses have two nearby zeros of the power associated with a π-jump of the phase.

With those typical experimental and numerical pictures in mind, we now study in detail the scenario implying the local formation of the Peregrine soliton that has been proposed to explain the emergence of heavy-tailed statistics in integrable turbulence[11,34].

Power and phase profiles of a typical structure recorded in experiments made with a 100-m-long PMF are plotted with a blue line in Fig. 4c,d together with plots made from the analytical formula characterizing the Peregrine soliton (black dashed line, see ref. [35]). The local intensity and phase profiles experimentally measured coincide well with those typifying the Peregrine soliton. In particular, one observes the characteristic π-phase jump at times where the optical power falls to zero. Our observation confirms the conclusion of previous studies that the Peregrine soliton represents a coherent structure of special importance in the context of integrable turbulence[11,12]. However, by putting together the temporal signatures of the phase and the power profiles (and not only the power), our experiments definitively demonstrate that the Peregrine soliton can locally emerge from the propagation of nonlinear random waves.

The knowledge of the phase and of the amplitude of the experimental field now opens the way to a full comparison between experiments and theory. In particular, as previously proposed in the context of experiments involving short pulses propagating in optical fibres[36] and of 2D experiments in photorefractive crystals[37], we can perform nonlinear digital holography. The idea is to use phase and amplitude profiles measured in the experiments as initial conditions in numerical simulations of 1D-NLSE. Numerical simulations can be performed either in the backward (reverse) direction or in the forward direction (for longer propagation than in the experiments). This technique gives access to the spatiotemporal dynamics inside the optical fibre.

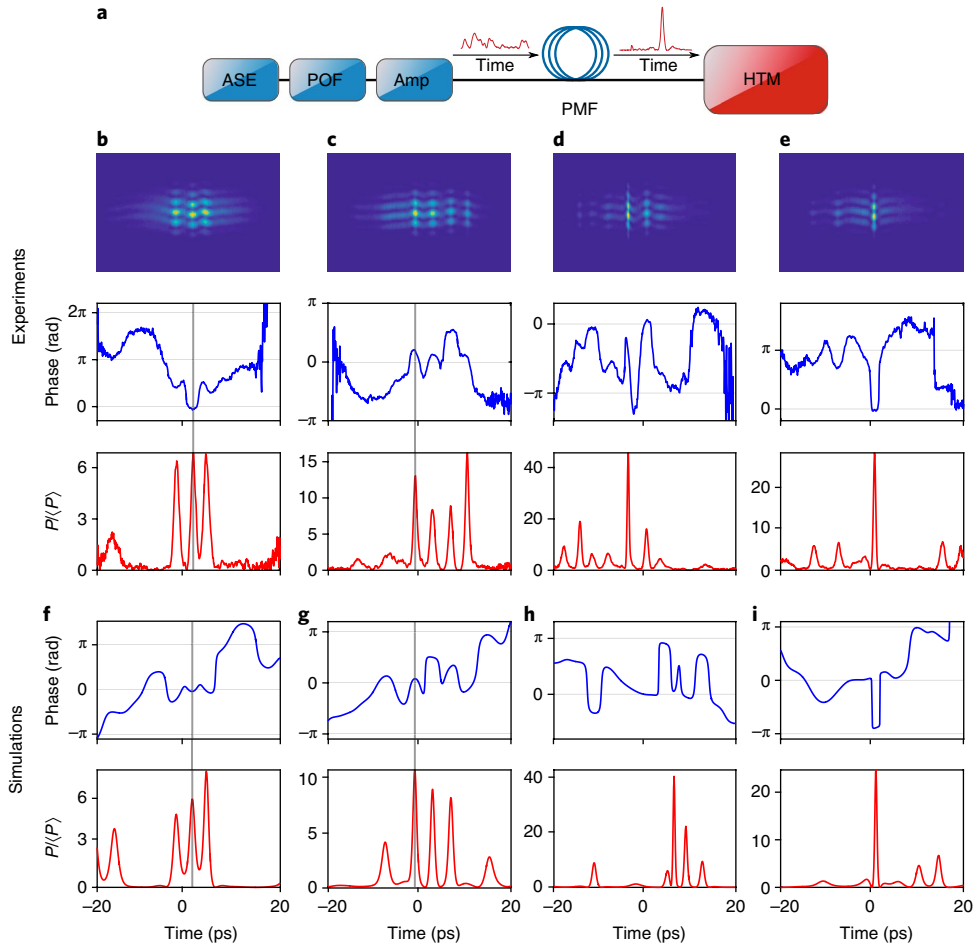

Fig. 3 | Nonlinear random waves. a, Experimental set-up. ASE, erbium fibre broadband amplified spontaneous emission source; POF, programmable optical filter to tailor the optical spectrum of the initial condition; AMP, erbium-doped fibre amplifier; PMF, 400-m-long polarization maintaining fibre; HTM, heterodyne time microscope shown in Fig. 1. **b**–**e**, Experiments. Typical raw images (top), retreived phase (middle) and optical power (bottom) of partially coherent waves after nonlinear propagation in a 400-m-long PMF. Note that the extrema of the phase and amplitude evolution often coincide (grey line in **b** and **c**). An example of extreme event (rogue wave) with a power of the order of 40 times the average power $\langle P\rangle$ is shown in **d**. Note also that **e** shows a structure similar to the Peregrine soliton (with π-jump of the phase at times where optical power falls to zero). **f**–**i**, Numerical simulations showing dynamical features similar to those revealed by experimental snapshots. Top, phase dynamics; bottom, optical power dynamics. In all cases, the initial spectral width of partially coherent waves is $\Delta\nu = 0.1$ THz. The mean optical power launched into the PMF is $\langle P\rangle = 2.6$ W.

We first use experimental data recorded at the output of the 100-m-long PMF (blue lines in Fig. 4a–d) as the initial condition in our numerical simulations. We have integrated numerically the 1D-NLSE from $z = 100$ m to $z = 0$ m and from $z = 100$ m to $z = 200$ m, where z is the propagation distance in the optical fibre. The spatiotemporal evolutions of the phase and amplitude obtained from numerical simulations are shown in Fig. 4a,b. The power and phase profiles computed from the 1D-NLSE at $z = 0$ m (see red line in Fig. 4e,f) reveal good qualitative agreement with the typical dynamics of the partially coherent waves launched inside the PMF and recorded with the HTM (see blue line in Fig. 4k,l). In particular, the field computed at $z = 0$ m exhibits random fluctuations with the expected timescale (~10 ps). The numerical integration of the 1D-NLSE between $z = 100$ m and $z = 200$ m shows that the Peregrine soliton-like structure observed in our experiment would split into two subpulses if nonlinear propagation was extended over another 100-m-long PMF.

Now, the phase and amplitude profiles that have been measured for the ASE light (blue line in Fig. 4k,l) are used as initial conditions for the numerical integration of the 1D-NLSE between $z = 0$ m and $z = 200$ m (see Fig. 4g,h). Numerical simulations reveal the growth of a Peregrine soliton-like structure that splits into two separate pulses after $z \cong 100$ m. Note that these spatiotemporal features are very similar to those typifying propagation of the so-called N-solitons[38] or of an isolated pulse in the strongly nonlinear regime (semiclassical limit of 1D-NLSE)[34,39] but here, they are found in the context of the propagation of partially coherent waves.

Digital focus option and SEAHORSE. As we are recording the full complex amplitude information, it is possible to skip the optional dispersive element placed on the signal path in the HTM. In this case, if we apply the same data processing as for the HTM, the retrieved signal $\psi_H(t)$ is no longer a replica of the random input signal $\psi(t)$, but rather it represents in the best situations a 'blurred' image of $\psi(t)$. However, it is possible to retrieve the input signal by using a strategy formally equivalent to the one used in digital holography. In digital holography, the object is recomposed numerically by applying an appropriate paraxial diffraction operator to the measured hologram[40]. In the SEAHORSE, the input signal $\psi(t)$ can be retrieved from the recorded hologram $\psi_H(t)$ by applying numerically a second-order dispersion operator characterized by a dispersion coefficient β corresponding exactly to the one of the removed

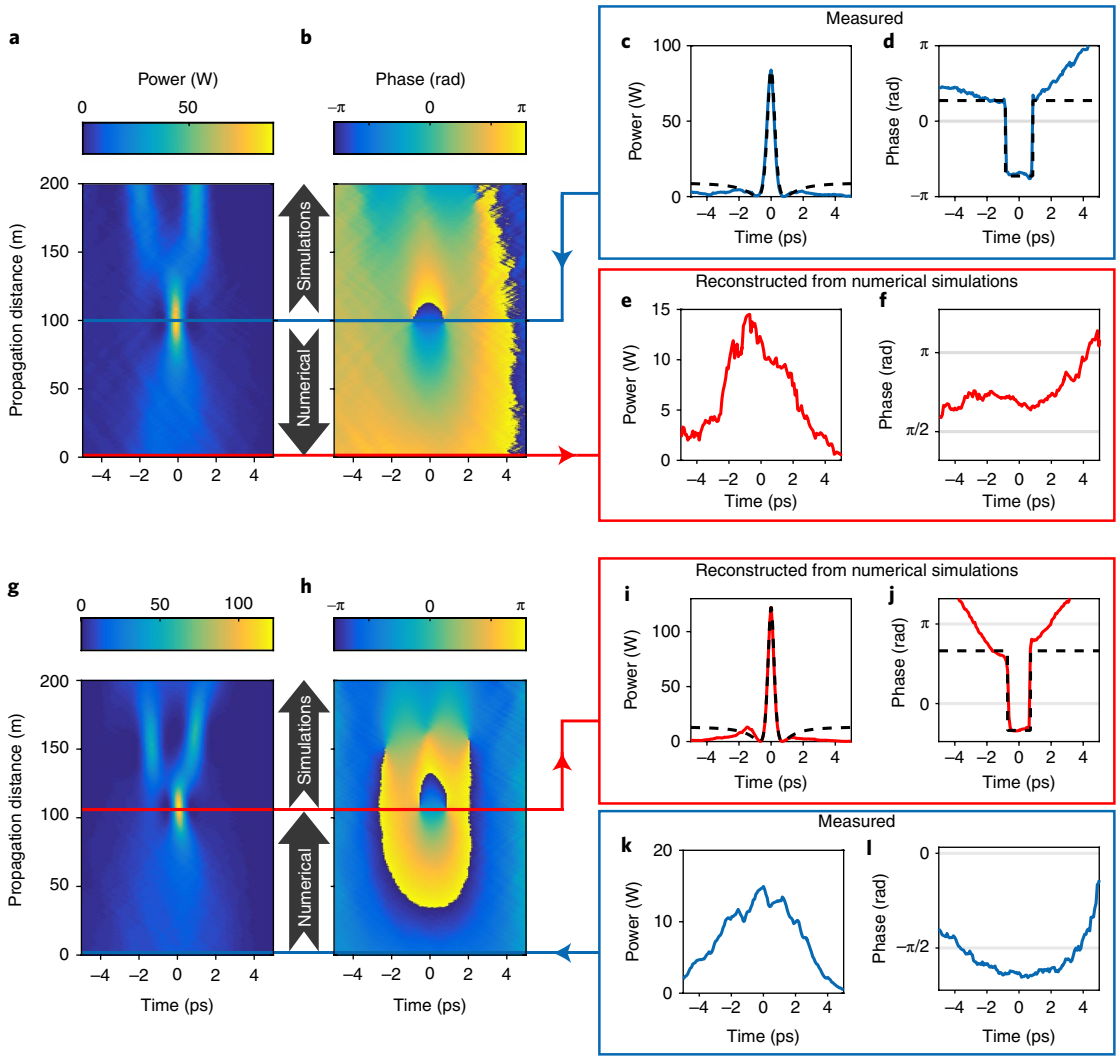

Fig. 4 | Nonlinear holography. a–**f**, Numerical simulations of 1D-NLSE using the experimental data recorded at the output of the 100-m-long PMF as the initial condition (blue line on **a** and **b**). Simulations are made in forward propagation direction (from 100 m to 200 m) and also in backward propagation direction (from 100 m to 0 m). **a**,**b**, Spatiotemporal evolution of the power (**a**) and of the phase (**b**). **c**,**d**, The evolution over time of the power (**c**) and phase (**d**) of the experimental data used as the initial condition. **e**,**f**, The evolution over time of the power (**e**) and of the phase (**f**) obtained at 0 m from numerical simulation in the backward propagation direction (red line on **a** and **b**). The dashed line is the analytical solution of the Peregrine soliton. **g**–**l**, Same as **a**–**f**, but the numerical simulation is made in the forward propagation direction (from 0 m to 200 m). **i**,**j**, The numerical result at 100 m. **k**,**l**, The initial experimental condition.

Treacy compressors (see Methods and Supplementary Video 2). In other words, in the SEAHORSE, the analog dispersion provided by the Treacy compressor of the HTM is replaced by digital dispersion.

By using the SEAHORSE, we have performed experiments involving nonlinear random waves identical to the ones made with the HTM. Remarkably, we have found phenomenological features similar to the one plotted in Fig. 4 (see Supplementary Information). Moreover, the statistical distributions of the nonlinear random waves recorded at the output of the PMF by using the HTM and the SEAHORSE are identical (see Supplementary Information).

We show now that the SEAHORSE allows the recording of signals with spectral width significantly larger than the one imposed by usual time imaging devices. We have recorded the hologram corresponding to two 80 fs pulses separated by ~2.7 ps (see Methods and Fig. 5a). As the spectrum of the two pulses is extremely broad (~15 THz), the 2D hologram (Fig. 5b) and the corresponding evolutions of the phase (Fig. 5c) and of the intensity (Fig. 5d) are rather complex. However, using a group velocity dispersion (GVD) coefficient $\beta = -0.21\,\mathrm{ps}^2$ that exactly corresponds to the dispersion previously induced by the Treacy compressor, the numerical propagation of the field leads to two extremely short peaks that are separated by 2.76 ps (Fig. 5e). Remarkably, the pulse width is ~80 fs, which corresponds to the distance between two pixels of the camera. This value can be considered as representing the temporal resolution of our temporal digital holography device (see Supplementary Information).

Relative performances of the two method variants (SEAHORSE and HTM) will deserve further investigations. As no dispersive system is needed on the signal path, SEAHORSE is a simpler device and has a better effective resolution (<100 fs) than the HTM (~200 fs, see Supplementary Information). The latter is limited by the aberrations induced by third-order dispersion of the Treacy compressor[41] (for the influence of aberrations in temporal imaging, see refs [20,42,43]). SEAHORSE holographic reconstruction thus represents a promising way to improve the resolution of time lenses, by strongly reducing the aberrations.

From a practical point of view, it is straightforward to visualize the phase and power evolutions from the raw camera images

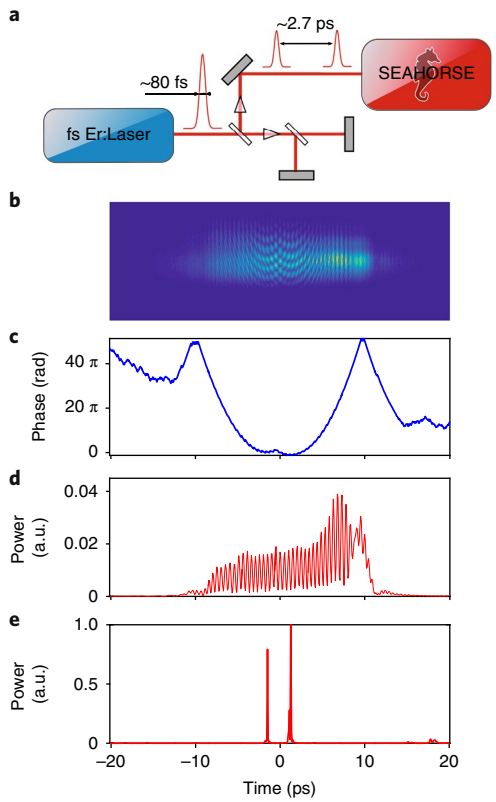

Fig. 5 | Digital time-holography set-up (SEAHORSE) and test data. **a**, Principle of the experimental test. A signal that is composed of two successive pulses with known delay is recorded by the SEAHORSE. **b**, Raw single-shot camera image. **c**,**d**, Corresponding evolutions of the phase (**c**) and power (**d**; see text for their precise meanings). **e**, Input signal retrieved from **c** and **d** using a digital holography algorithm (see text and Methods).

provided by the HTM, whereas SEAHORSE requires more complex data analysis. No artefact induced by the retrieval algorithm of SEAHORSE has been noticed in our experiments. However as the measurements of phase and amplitude are coupled in SEAHORSE (and not in HTM), the phase may be more affected by the amplitude noise, in particular when examining low power input data. The comparison of signal noise ratio in HTM and SEAHORSE will require specific works.

Discussion

In this study, we have demonstrated two novel and complementary techniques that allow the single-shot recording of amplitude and phase of irregular waves with a high temporal resolution (~80 fs for the SEAHORSE) over a long time window (~40 ps). The key point is a completely new combination of the heterodyne technique[3,22] and of the so-called time-lens strategy that provide large temporal windows[11,12,17].

We believe that our devices represent complementary tools to single-shot versions of fast-detection devices such as FROG[2] or SPIDER[44] in the studies of complex and non-reproducible optical signals. In particular, one of the key advantages of the HTM and of the SEAHORSE is the combination of large temporal window recorded in single shot together with subpicosecond resolution. These new devices allow the study of continuously emitted random waves that require temporal gating (provided here by the chirped pulse of the time lens). In the set-up of single-shot XFROG[9], few picosecond pulses can be recorded whereas hundred of picoseconds can potentially be recorded with a time lens. Among the existing techniques, SPIDER with external chirped pulse[45] also provides a natural gating, but the necessary interaction with a monochromatic wave restricts the measurement to very short pulses (typically 10–100 fs)[46].

From a general point of view, the different types of FROG, SPIDER and other spectral interferometric devices such as SEA-TADPOLE[4] have paved the way for the measurement of ultrafast laser pulses[2,46]. Very recently, it has been demonstrated that the complex phase and amplitude dynamics of mode-locked lasers can also be measured in real-time by the simultaneous use of dispersive Fourier transform and time-lens techniques[14]. We believe that the HTM and the SEAHORSE now open the way to the experimental study of randomly fluctuating continuous optical waves.

From a fundamental point of view, the HTM and the SEAHORSE have unveiled the special evolution of the phase (and amplitude) of rogue waves in integrable turbulence, and in particular their compatibility with the expected Peregrine soliton[34,35,47,48]. Our results open the way to novel and fundamental investigations of nonlinear propagation of random waves, of the emergence of optical rogue waves[10–12,32,33,49] and more generally of the field of nonlinear statistical optics[50].

Methods

Methods, including statements of data availability and any associated accession codes and references, are available at https://doi.org/10.1038/s41566-018-0113-8.

Received: 24 July 2017; Accepted: 24 January 2018;
Published online: 12 March 2018

References

1. Reid, D. T. et al. Roadmap on ultrafast optics. *J. Opt.* **18**, 093006 (2016).
2. Trebino, R. *Frequency-Resolved Optical Gating: The Measurement of Ultrashort Laser Pulses* (Springer Science and Business Media, New York, 2012).
3. Broaddus, D. H., Foster, M. A., Kuzucu, O., Koch, K. W. & Gaeta, A. L. Ultrafast, single-shot phase and amplitude measurement via a temporal imaging approach. In *Conference on Lasers and Electro-Optics* CMK6 (Optical Society of America, 2010).
4. Bowlan, P. et al. Crossed-beam spectral interferometry: a simple, high-spectral-resolution method for completely characterizing complex ultrashort pulses in real time. *Opt. Express* **14**, 11892–11900 (2006).
5. Alonso, B. et al. Spatiotemporal amplitude-and-phase reconstruction by Fourier-transform of interference spectra of high-complex-beams. *J. Opt. Soc. Am. B.* **27**, 933–940 (2010).
6. Mahjoubfar, A. et al. Time stretch and its applications. *Nat. Photon.* **11**, 341–351 (2017).
7. Rhodes, M., Steinmeyer, G. & Trebino, R. Standards for ultrashort-laser-pulse-measurement techniques and their consideration for self-referenced spectral interferometry. *Appl. Opt.* **53**, D1–D11 (2014).
8. Wetzel, B. et al. Real-time full bandwidth measurement of spectral noise in supercontinuum generation. *Sci. Rep.* **2**, 882 (2012).
9. Wong, T. C., Rhodes, M. & Trebino, R. Single-shot measurement of the complete temporal intensity and phase of supercontinuum. *Optica* **1**, 119–124 (2014).
10. Solli, D. R., Ropers, C., Koonath, P. & Jalali, B. Optical rogue waves. *Nature* **450**, 1054–1057 (2007).
11. Suret, P. et al. Single-shot observation of optical rogue waves in integrable turbulence using time microscopy. *Nat. Commun.* **7**, 13136 (2016).
12. Närhi, M. et al. Real-time measurements of spontaneous breathers and rogue wave events in optical fibre modulation instability. *Nat. Commun* **7**, 13675 (2016).
13. Herink, G., Kurtz, F., Jalali, B., Solli, D. R. & Ropers, C. Real-time spectral interferometry probes the internal dynamics of femtosecond soliton molecules. *Science* **356**, 50–54 (2017).
14. Ryczkowski, P. et al. Real-time full-field characterization of transient dissipative soliton dynamics in a mode-locked laser. *Nat. Photon.* https://doi.org/10.1038/s41566-018-0106-7 (2018).
15. Picozzi, A. Towards a nonequilibrium thermodynamic description of incoherent nonlinear optics. *Opt. Express* **15**, 9063–9083 (2007).
16. Turitsyna, E. G. et al. The laminar-turbulent transition in a fibre laser. *Nat. Photon.* **7**, 783–786 (2013).
17. Kolner, B. H. & Nazarathy, M. Temporal imaging with a time lens. *Opt. Lett.* **14**, 630–632 (1989).
18. Foster, M. A. et al. Silicon-chip-based ultrafast optical oscilloscope. *Nature* **456**, 81–84 (2008).

19. Bennett, C. & Kolner, B. Upconversion time microscope demonstrating 103× magnification of femtosecond waveforms. *Opt. Lett.* **24**, 783–785 (1999).
20. Salem, R., Foster, M. A. & Gaeta, A. L. Application of space–time duality to ultrahigh-speed optical signal processing. *Adv. Opt. Photon.* **5**, 274–317 (2013).
21. Kauffman, M., Banyai, W., Godil, A. & Bloom, D. Time-to-frequency converter for measuring picosecond optical pulses. *Appl. Phys. Lett.* **64**, 270–272 (1994).
22. Dorrer, C. Single-shot measurement of the electric field of optical waveforms by use of time magnification and heterodyning. *Opt. Lett.* **31**, 540–542 (2006).
23. Dorrer, C. Electric field measurement of optical waveforms. US patent 7,411,683 (2008); https://www.google.com/patents/US7411683
24. Kosik, E. M., Radunsky, A. S., Walmsley, I. A. & Dorrer, C. Interferometric technique for measuring broadband ultrashort pulses at the sampling limit. *Opt. Lett.* **30**, 326–328 (2005).
25. Wyatt, A. S., Walmsley, I. A., Stibenz, G. & Steinmeyer, G. Sub-10 fs pulse characterization using spatially encoded arrangement for spectral phase interferometry for direct electric field reconstruction. *Opt. Lett.* **31**, 1914–1916 (2006).
26. Kreis, T. Digital holographic interference-phase measurement using the Fourier-transform method. *J. Opt. Soc. Am. A* **3**, 847–855 (1986).
27. Walczak, P., Randoux, S. & Suret, P. Optical rogue waves in integrable turbulence. *Phys. Rev. Lett.* **114**, 143903 (2015).
28. Agafontsev, D. & Zakharov, V. E. Integrable turbulence and formation of rogue waves. *Nonlinearity* **28**, 2791 (2015).
29. Soto-Crespo, J. M., Devine, N. & Akhmediev, N. Integrable turbulence and rogue waves: Breathers or solitons? *Phys. Rev. Lett.* **116**, 103901 (2016).
30. Randoux, S., Gustave, F., Suret, P. & El, G. Optical random riemann waves in integrable turbulence. *Phys. Rev. Lett.* **118**, 233901 (2017).
31. Zakharov, V. E. Turbulence in integrable systems. *Stud. Appl. Math.* **122**, 219–234 (2009).
32. Akhmediev, N., Ankiewicz, A. & Taki, M. Waves that appear from nowhere and disappear without a trace. *Phys. Lett. A* **373**, 675–678 (2009).
33. Akhmediev, N., Soto-Crespo, J. SpringerAmpamp; Ankiewicz, A. Extreme waves that appear from nowhere: on the nature of rogue waves. *Phys. Lett. A* **373**, 2137–2145 (2009).
34. Bertola, M. & Tovbis, A. Universality for the focusing nonlinear Schrödinger equation at the gradient catastrophe point: rational breathers and poles of the tritronquée solution to Painlevé i. *Comm. Pure Appl. Math.* **66**, 678–752 (2013).
35. Kibler, B. et al. The peregrine soliton in nonlinear fibre optics. *Nat. Phys.* **6**, 790–795 (2010).
36. Tsang, M., Psaltis, D. & Omenetto, F. G. Reverse propagation of femtosecond pulses in optical fibers. *Opt. Lett.* **28**, 1873–1875 (2003).
37. Barsi, C., Wan, W. & Fleischer, J. W. Imaging through nonlinear media using digital holography. *Nat. Photon.* **3**, 211–215 (2009).
38. Agrawal, G. P. *Nonlinear Fiber Optics: Optics and Photonics* 3rd edn (Academic Press, San Diego, 2001).
39. Tikan, A. et al. Universality of the Peregrine soliton in the focusing dynamics of the cubic nonlinear Schrödinger equation. *Phys. Rev. Lett.* **119**, 033901 (2017).
40. Schnars, U. & Jüptner, W. *Digital Holography: Digital Hologram Recording, Numerical Reconstruction, and Related Techniques* (Springer Science and Business Media, Berlin, 2005).
41. Backus, S., Durfee, C. G. III, Murnane, M. M. & Kapteyn, H. C. High power ultrafast lasers. *Rev. Sci. Instrum.* **69**, 1207–1223 (1998).
42. Bennett, C. V. *Parametric Temporal Imaging and Aberration Analysis*. PhD thesis, Univ. California (2000).
43. Bennett, C. V. & Kolner, B. H. Aberrations in temporal imaging. *IEEE J. Quantum Electron.* **37**, 20–32 (2001).
44. Dorrer, C. et al. Single-shot real-time characterization of chirped-pulse amplification systems by spectral phase interferometry for direct electric-field reconstruction. *Opt. Lett.* **24**, 1644–1646 (1999).
45. Hirasawa, M. et al. Sensitivity improvement of spectral phase interferometry for direct electric-field reconstruction for the characterization of low-intensity femtosecond pulses. *Appl. Phys. B* **74**, s225–s229 (2002).
46. Walmsley, I. A. & Dorrer, C. Characterization of ultrashort electromagnetic pulses. *Adv. Opt. Photon.* **1**, 308–437 (2009).
47. Dudley, J. M., Dias, F., Erkintalo, M. & Genty, G. Instabilities, breathers and rogue waves in optics. *Nat. Photon.* **8**, 755–764 (2014).
48. Toenger, S. et al. Emergent rogue wave structures and statistics in spontaneous modulation instability. *Sci. Rep.* **5**, 10380 (2015).
49. Mussot, A. et al. Observation of extreme temporal events in CW-pumped supercontinuum. *Opt. Express* **17**, 17010–17015 (2009).
50. Picozzi, A. et al. Optical wave turbulence: towards a unified nonequilibrium thermodynamic formulation of statistical nonlinear optics. *Phys. Rep.* **542**, 1–132 (2014).

Acknowledgements

This work has been partially supported by the Agence Nationale de la Recherche through the LABEX CEMPI project (ANR-11-LABX-0007) and by the Ministry of Higher Education and Research, Hauts-de-France Regional Council and European Regional Development Fund (ERDF) through the Contrat de Projets Etat-Région (CPER Photonics for Society P4S) and by the Centre National de la Recherche Scientifique (CNRS) through the project MICRO TURBU. The authors thank A. Mussot, the photonics group of the PhLAM and P. Szriftgiser for fruitful discussions and technical help. The authors also acknowledge MENLO for providing the femtosecond laser used for the time-holography measurements. The authors thank N. Savoia for the everyday work on the femto laser and R. El Koussaifi, C. Evain and M. Le Parquier for their crucial contribution in the development of the time lens.

Author contributions

All authors contributed to the design and the realization of the heterodyne time microscope and time-holography devices. All the authors participated in the data acquisition that has been essentially performed by A.T. All authors participated in data analysis, numerical simulations and have written the manuscript.

Competing interests

The authors declare no competing interests.

Additional information

Supplementary information is available for this paper at https://doi.org/10.1038/s41566-018-0113-8.

Reprints and permissions information is available at www.nature.com/reprints.

Correspondence and requests for materials should be addressed to P.S.

Publisher's note: Springer Nature remains neutral with regard to jurisdictional claims in published maps and institutional affiliations.

Methods

Heterodyne time microscope. For the single-shot acquisition of phase and amplitude of subpicosecond optical fields, the heterodyne technique is implemented in an upconversion time-microscope composed[19] of a time lens and a single-shot spectrometer very similar to the one described in ref. [11]. A reference monochromatic local oscillator with a wavelength of ~1,561 nm close to the one of the signal under investigation is superimposed on the signal (see Fig. 1). Without this reference continuous-wave (CW) signal, the system is a time microscope, which produces a 'spatial replica' (at a central wavelength $\lambda_{vis} \cong 529$ nm) of the signal power evolution onto the horizontal axis of the camera[11].

The HTM encodes the temporal change of an interference pattern onto the spectrum of a chirped pulse. The fringe pattern is imaged onto the vertical axis of a sCMOS camera and the spectrum is imaged on the horizontal axis of the camera using a 1,800 lines mm^{-1} grating. The camera is a sCMOS Hamamatsu Orca flash 4.0 V3 (C13440-20CU). By using a region of interest with a size of 512 × 100 pixels, the repetition rate of the camera used with CameraLink and external trigger can be greater than 10^3 frames s^{-1}. In our experiments, the 2D pattern is therefore recorded in single shot with 512 × 100 pixels at the repetition rate of the 800 nm pump laser (1 kHz).

We use an upconversion time lens as in ref. [17] (see Fig. 1). A 1-mm-long BBO crystal cut for noncollinear type-I SFG is pumped by 800 nm chirped pulses that are provided by an amplified titanium-sapphire laser (Spitfire from Spectra Physics). The laser emits 2 mJ, 40 fs pulses with a spectral bandwidth of about 25 nm at 1 kHz repetition rate, and only 20 µJ are typically used here. For inducing the required normal dispersion on the 800 nm pulses, we simply adjust the amplifier's output compressor dispersion. The dispersion was fixed to 0.21 ps^2, leading to chirped pulses with a duration of about 25 ps.

Before being focused inside the BBO crystal, the 1,561 nm signal under investigation experiences anomalous dispersion in a classic Treacy grating compressor (see Fig. 1). The 1,561 nm grating compressor is made with two 600 lines mm^{-1} gratings, operated at an angle of incidence of 49°, and whose planes are separated by 38.5 mm. The signal is then combined with the single-frequency reference beam at 1,561 nm by using a non-polarizing cube. The single-frequency reference beam is emitted by a tunable laser source with a narrow linewidth of ~300 kHz (APEX AP3350A). The coherence timescale of the reference source (~3 µs) is much higher than the temporal windows of recording (~40 ps) so that the phase of the reference can be considered as being constant over each observation window. The reference light is amplified by using an erbium-doped fibre amplifier (Keopsys) to a power of a few watts.

The 800 nm beam, the reference beam and the signal beam are designed to assume a transverse elliptic shape by using cylindrical lenses. The horizontal waist diameter of the three beams is typically 50 µm. The vertical waist of the 1,561 nm beams is typically 500 µm and the vertical waist of the 800 nm beam is typically 1 mm.

All optical paths are horizontal, except the CW local oscillator signal which enters the BBO crystal with a small angle α with respect to the horizontal plane, as shown in Fig. 1b. This angle of ~10 mrad between the signal under investigation and the monochromatic reference is adjusted in the vertical plane to obtain several horizontal interference fringes in the observation plane.

To reject the 800 nm and 1,561 nm radiations and to illuminate the camera with only the SFG at 529 nm, an iris and a 40 nm bandpass filter around 531 nm (FF01 531/40-25 Semrock) are placed after the crystal. An achromatic lens with 200 mm focal length collimates the 529 nm light after the BBO crystal. The camera is a sCMOS Hamamatsu Orca flash 4.0 V3 (C13440-20CU), equipped with a 60 mm lens (Nikkor Micro 60 mm f/2.8 AF-D). The objective is focused at infinity and the waist of the SFG light in the BBO crystal is imaged on the camera sensor. The camera is synchronized on the 800 nm laser pulses, and the integration time is adjusted to 1 ms, thus enabling single-shot operation of the time microscope.

As in other time-lens systems[17–19] high resolution requires proper adjustment of the dispersion produced by the 1,561 nm compressor. This is conceptually analogous to the focus that is required in a conventional microscope, and performed by adjusting the object–objective distance. We adjust the distance between the two gratings of the Treacy compressor by minimizing the width of the image of femtosecond pulses (see ref. [11] for the details of the procedure). The best temporal resolution is achieved for a dispersion value of $\beta \simeq -0.21$ ps^2. This value is very close to the theoretical expectation, that is, exactly opposite to dispersion experienced by the 800 nm pulse. For all results presented in this study, the temporal resolution of the HTM is 200 fs full width at half maximum, and the field of view is around 40 ps. Note that in spatial imaging, the diffraction induced by the free propagation from the focal plane to the lens is compensated by the quadratic phase of the lens. Equivalently, in time-lens devices based on SFG, the group velocity dispersions experienced by the pump and by the signal need to have opposite signs to somehow compensate mutually[42]. In our device, normal dispersion was easily achieved for the pump pulse by detuning the compressor provided together with the titanium-sapphire amplifier and anomalous dispersion was achieved by using a Treacy compressor for the signal.

Partially coherent light. The partially coherent light used in the experiments reported in Fig. 2 is generated by an erbium fibre broadband ASE source (TBS-S130 from BKTEL Photonics). This broadband light is spectrally filtered (with programmable shape and linewidth) using a programmable optical filter (Waveshaper 1000S, Finisar). The filtered light is then amplified by using an erbium-doped fibre amplifier (Keopsys). In the experiments reported in Fig. 3, the partially coherent light obtained in this way is launched inside a single-mode PMF (Fibercore HB-1550T), with either 100 m or 400 m length. The measured group velocity (second order) dispersion coefficient of the fibre is $\beta_2 = -22$ ps^2 km^{-1}. For a given spectral width, the power of the light beam launched inside the fibre is controlled using a half-wavelength plate and a polarizing cube.

Time calibration of the HTM. Time calibration of the HTM is performed by using a series of two laser pulses that are separated by a well-calibrated time delay. The pulses are emitted by a 1.5 µm mode-locked laser (from Pritel) and have ~1 ps temporal width. Those laser pulses propagate inside the PMF where they experience differential group delay depending on their state of polarization. The time separation (5.6 ps) between the two pulses is accurately measured from spectral interferometry. Observation of the two pulses on the sCMOS camera then permits the accurate calibration of the time axis and to measure that one camera pixel corresponds to a time duration of 79 fs.

Data processing-phase and power measurement. The intensity $I(x, y)$ along one vertical line y at the position x is given by the beating between the signal beam and the reference beam. It can be presented in the form:

$$\begin{aligned} I(x,y) &= I_r(x,y) + I_s(x,y) \\ &+ 2\sqrt{I_r(x,y)I_s(x,y)}\cos[k_y y + \phi(x)] \end{aligned} \quad (1)$$

$I_r(x, y)$ represents the transverse intensity profile that would be detected by the sCMOS camera in absence of the signal beam and $I_s(x, y)$ represents the transverse intensity profile that would be detected by the sCMOS camera in absence of the reference beam. $2\pi/k_y$ is the spatial period along a vertical line of the interference pattern observed with the sCMOS camera.

In the analysis presented in this study, we neglect the power fluctuations of the reference laser. We thus compute $I_r(x, y)$ from additional experiments in which we record the signal arising from the SFG between the pump and the reference beams (without the signal).

In the experiments, we have chosen the angle between the reference and the signal beams to oberve a sufficiently large number of fringes so that $\int \sqrt{I_r(x,y)\,.\,I_s(x,y)}\cos[k_y y + \phi(x)]\,dy \simeq 0$. For each frame, we thus simply compute the optical power $P(x)$ of the signal by using the formula:

$$P(x) = \int I(x,y)\mathrm{d}y - \int I_r(x,y)\mathrm{d}y \quad (2)$$

Note that here P has arbitrary units. In our study about partially coherent waves (Figs. 2–4), we compute the average $\langle P(x)\rangle$ from 5×10^4 frames. We then display $P(x)/\langle P(x)\rangle$ or $[P(x)/\langle P(x)\rangle] \times P_0$ where P_0 is the averaged power launched inside the fibre. We remind that one pixel in x corresponds to 79 fs. The full width at half maximum of $\langle P(x)\rangle$ corresponds to a temporal width 25 ps that is close to the duration of the chirped pump pulse. The division by $\langle P(x)\rangle$ extends the window of observation to typically 40 ps (see Supplementary Information).

In the study of the optical spectra of partially coherent waves (Fig. 2), the procedure described above is first applied (division by $\langle P(x)\rangle$). Then we multiply the window by an hyper Gaussian $\exp(-[t^2/(2\Delta t^2)]^{15})$ with $\Delta t = 12$ ps to achieve zero boundary conditions on the sides of the window. This allows the computation of the Fourier spectrum by using the standard fast Fourier transform (FFT) algorithm.

The relative phase between the signal and the reference $\phi(x)$ is simply given by the position of the maxima of the interference fringes (see equation (1)). $\phi(x)$ can be easily determined by the FFT of $I(x, y)$ in the variable y. $\phi(x)$ is given by the phase (complex argument) of the isolated spectral peak associated with the pattern that oscillates at the frequency k_y along the y direction[26].

Time holography. In our time holography set-up, the signal under interest no longer experiences dispersion by being injected into the Treacy compressor. In a conventional microscope, this amounts to placing the object under study very close to the microscope objective. With this change, we record the complex field $\psi_H(t)$ associated with the temporal hologram instead of the temporal image of the signal under investigation.

The time evolution of the signal under investigation $\psi(t)$ can be obtained by applying an appropriate dispersion operator in the Fourier space, that is:

$$\tilde{\psi}(\omega) = \tilde{\psi}_H(\omega)\mathrm{e}^{-i\beta\omega^2/2} \quad (3)$$

where $\tilde{\psi}_H(\omega)$ and $\tilde{\psi}(\omega)$ are the Fourier transforms of $\psi_H(t)$ and of $\psi(t)$, respectively. ω is the pulsation of the complex optical field envelop and β is a dispersion coefficient. From the theoretical point of view, the value of β must be exactly equal to the opposite of the GVD characterizing the chirped pump pulse used in the time lens, that is $\beta = -0.21$ ps^2.

The pair of ultrashort pulses used to demonstrate the capabilities of the time holography is produced by a femtosecond erbium laser (ELMO, from Menlo Systems) equipped with a Michelson interferometer. The output pulse duration at the 1,553 nm central wavelength is ≤80 fs and the repetition rate is 100 MHz. The energy of one pulse launched in the BBO crystal is typically ~0.2 nJ. To create the double pulse signal, we used a Michelson interferometer with tunable optical path difference. We fixed the delay between two pulses at the value ~2.7 ps (measured with the full HTM including the Treacy compressor).

Numerical simulations of the 1D-NLSE. Numerical simulations presented in Figs. 3 and 4 are performed by integrating the 1D-NLSE:

$$i\frac{\partial\psi}{\partial z} = -\frac{\beta_2}{2}\frac{\partial^2\psi}{\partial t^2} + \gamma\,|\psi|^2\,\psi \tag{4}$$

ψ represents the complex envelope of the electric field, normalized so that $|\psi|^2$ is the optical power. z is the longitudinal coordinate measured along the fibre and t is the retarded time. $\beta_2 = -22\,\mathrm{ps^2\,km^{-1}}$ is the second-order dispersion coefficient of the fibre and γ is the Kerr coupling coefficient. From the comparison between the optical spectra measured in the experiments and the ones computed from the numerical simulations, we estimate that the Kerr coefficient is $\gamma \cong 2.4\,\mathrm{W^{-1}\,km^{-1}}$. All numerical integrations are performed using splitstep pseudospectral methods.

In the numerical simulations presented in this study, we neglect linear losses (≃0.5 dB in the 400-m-long PMF) and stimulated Raman scattering. These approximations provide precise and quantitative agreement between experiments and numerical simulations at moderate powers (<2 W).

Data availability. The data that support the plots within this paper and other findings of this study are available from the corresponding author upon reasonable request.